RSC Advances

PAPER



Cite this: *RSC Adv.*, 2024, **14**, 24791

# Ferritin cages as building blocks for higher-order assembly through copper–sulfur bonds for HER analysis†

Ruoxuan Sun and Sierin Lim *

Received 20th April 2024
Accepted 30th May 2024

DOI: 10.1039/d4ra02931c

rsc.li/rsc-advances

Higher-order assembly of ferritins has been achieved on copper substrate by introducing cysteines on their surfaces with thiol groups as the active moiety. To elucidate the assembly mechanism, Raman spectroscopy was utilized to characterize the interaction between the copper substrate and the modified ferritin, AfFtnAA/E94C. The resulting higher-order architecture shows enhanced hydrogen evolution reaction activity.

## Introduction

Natural macromolecules play an essential role in biological systems and are capable of dynamically and exclusively interacting and assembling to produce fine-functioning systems with accuracy, efficiency, and adaptability.[1] As one of the vital constituents of natural macromolecules, proteins naturally possess the ability to assemble into different patterns, conferring various functions to the physical and biological processes they are involved in. Inspired by nature, protein-based superstructures have received extensive research interest due to their biocompatibility and chemical versatility.[2] Another important advantage of constructing higher-order structures based on proteins is flexibility. By varying the components, structures, and conditions of the assembly, the physiochemical properties of the material can be tuned.[3] Utilizing chemical alteration, biotechnologies, or the combination of both strategies, modifications have been applied to construct versatile protein assemblies.[4] Proteins, as building blocks, have been assembled into superstructures *via* various methods.[1,2] These proteins are typically monomeric – a single subunit as the building block. However, within the protein-based architectures, limited research has been reported in the context of assemblies based on multimeric proteins, such as protein cages where multiple subunits serve as the bulding blocks.

Protein cages have been proposed as building blocks for building higher-order structures owing to their structural consistency after encapsulation, modification, or assembly with expandable functionalities across multiple length scales.[4] Protein cages are robust with symmetrical architectures comprising different numbers of subunits.[4] Among all categories of proteins, cage-like proteins have directed considerable research attention due to their versatile functions, including iron storage and mineralization of ferritins,[5] encapsidation and transportation of the genome of viral capsids,[6] and regulatory role of heat shock proteins.[7] In addition, diverse functional groups on amino acid chains of protein cages offer more possibility for introducing varied interactions for distinct assemblies.[8] The structure of protein cages is defined and the interfaces of protein cages, including the exterior surface, the interior surface, and the interface between subunits of protein cages, provide possibilities for adding new elements to individual cages and for further bestowing non-natural functionalities.[9] Moreover, protein cages serve as a flexible element for assembly. The subunits of a protein cage are capable of assembling to a cage-like structure, and individual protein cages can further act as building blocks for higher-order structures.[4] Despite the superior characteristics of protein cages, the intolerance of high temperature is a typical limitation of biological constituents of the synthesis of artificial materials.[5] Among all protein cages, ferritin has two important features that are thermostability of up to 80 °C and specific denaturant-stability.[10] Ferritins are iron storage proteins with a highly conserved structure, comprising of usually 24 subunits.[11] Thus, benefiting from these advantages, protein cages are considered favorable building blocks for fabricating higher-order architectures.

Studies have been carried out using protein cages as building blocks to assemble into superstructures *via* various methods. These include electrostatic interactions[12–16] and metal–ligand coordination.[17–19] More interactions can be designed to drive the construction of architectures based on protein cages. Much uncertainty still exists since systematic exploration of this field is lacking. Moreover, individual protein cages have been adopted to design a wide range of materials for multiple applications, such as drug delivery,[20] vaccine,[21] and cosmetic.[22] Despite utilizing the protein cage as an entity in applications, the exploration of functional aspects of protein-cage-based architectures is limited. While a few achievements have been

*School of Chemistry, Chemical Engineering and Biotechnology, Nanyang Technological University, 70 Nanyang Drive, 637457, Singapore. E-mail: slim@ntu.edu.sg*

† Electronic supplementary information (ESI) available. See DOI: https://doi.org/10.1039/d4ra02931c

attained in the functional characterization of protein-cage-based assemblies including mechanical behaviors,[23] thermo-mechanical properties,[24] and drug encapsulation,[25] electro-catalytic behaviors of protein-cage-based assemblies, such as electrocatalytic hydrogen evolution reaction (HER) performances, remain obscure. Electrocatalytic HER is one of the essential steps of electrochemical water splitting, thus, the optimization of HER activity has emerged as an important topic for future energy supply owing to the clean and renewable feature of hydrogen fuel,[26] which has high energy (142 kJ $g^{-1}$) and green burning end product, water.[27] Therefore, exploration of HER performance of protein-cage-based assemblies is appealing and challenging.

Herein, we report an approach for assembling higher-order protein structures on copper substrate using ferritin as building blocks by the single point mutation on the external surface of ferritin cages (Fig. 1). Further characterization was conducted to investigate the morphology, the assembly mechanism, and HER performances of this structure. This work explores development of functional biomaterials with protein cages as the building blocks.

## Results and discussion

### Mutant design

In this study, the mutant of *Archaeoglobus fulgidus* ferritin (AfFtn), AfFtnAA/E94C, was selected as the building block. Substitution of lysine 150 (K150) and arginine 151 (R151) of AfFtn with alanine enhanced hydrophobic interactions at surfaces around the 4-fold (C4) axes and resulted a closed octahedral cage, AfFtnAA, which is thermally more stable.[28] Compared with other ferritins, the self-assembly and disassembly of subunits of AfFn and AfFtnAA can be tuned by salt and metal concentration in mild conditions, showing potential applications in biomedical fields.[29] Ascribing to the rarity and high reaction activity towards multiple reagents, cysteine is a commonly applied targeting spot for further manipulation of protein-based materials.[2] Upon inspection, we replaced the glutamic acid at position 94 (E94) with cysteine to enable subsequent higher-order construction. E94 is located on the outer surface of the ferritin cage far from the C4 axis of the cage. This selection will avoid pore opening after modification at the K150 and R151 positions. The cysteine residues introduced on the surface of AfFtnAA/E94C provide thiol groups for bonding to copper substrate. Since only one cyctein was introduced to each subunit and 24 subunits assemble to form a protein cage, 24 cystein residues on each cage are expected to be available for interactions with the copper substrate.

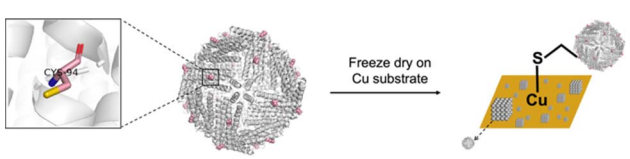


Fig. 1 Schematic diagram of the assembly of cysteine-modified ferritin cages *via* copper template manipulation.

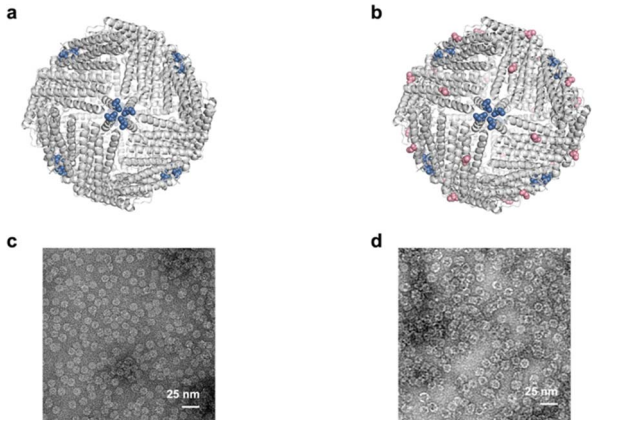


Fig. 2 (a and b) Ribbon diagrams of (a) AfFtnAA and (b) AfFtnAA/E94C. K150 and R151 are shown in blue and C94 of AfFtnAA/E94C are shown in red. (c) TEM image of AfFtnAA. (d) TEM image of AfFtnAA/E94C.

### AfFtnAA/E94C expression and purification

The Cys94 of AfFtnAA/E94C located at the exterior surface of ferritin cages is visualized using PyMol (Fig. 2b). AfFtnAA/E94C was overexpressed in *E. coli* and purified by column chromatography following previously reported method.[30] During the process of hydrophobic interaction chromatography (HIC), one main peak was collected (Fig. S1b†). The purity of the peak, which was expected to correspond to AfFtnAA/E94C, was confirmed by sodium dodecyl sulphate-polyacrylamide gel electrophoresis (SDS-PAGE) (Fig. S1d†). The single thick band at around 20 kDa on the SDS-PAGE shows that AfFtnAA/E94C was efficiently produced in *E. coli* BL21(DE3)C+RIL and purified. The dynamic light scattering (DLS) results demonstrate that the diameter is about ~18 nm, similar to the iron-loaded AfFtn and AfFtnAA (Fig. S1f†). The molecular mass measured by matrix-assisted laser desorption/ionization time-of-flight (MALDI-TOF) mass spectrometry corresponds to the theoretical molecular mass of AfFtnAA/E94C of ~20 kDa (Fig. S1h†). Transmission electron microscopy (TEM) image of AfFtnAA/E94C (Fig. 2d) shows the intact and hollow monodispersed cage structure, which is consistent with previous work.[30] These results indicate the effective and successful preparation of AfFtnAA/E94C building blocks for further interaction with copper substrate to construct higher-order structures. AfFtnAA illustrated in Fig. 2a was expressed and purified as the control following similar approach.[30] The characterizations are shown in Fig. S1a, e, g and S2a.†

### Morphology characterizations of AfFtnAA/E94C assembly

Using AfFtnAA/E94C as building blocks, the assembly of higher-order structures on the copper substrate was conducted by freeze drying. The morphology was examined by field emission scanning electron microscopy (FESEM) and atomic force microscopy (AFM). The SEM images of samples at different concentrations demonstrated a process of how the increase in concentration alters the structure of the assembly. Protein cages initially aggregated into small fractions at low concentration

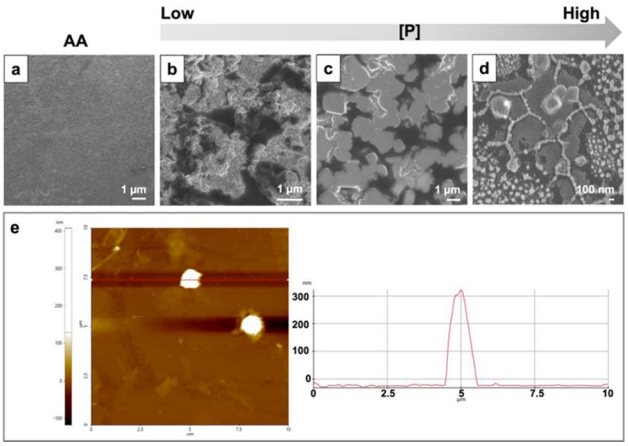


Fig. 3 Morphologies of the assembly of AfFtnAA/E94C at different concentrations on Cu substrate *via* freeze drying method. (a) SEM image AfFtnAA serving as the control group. (b and d) SEM image on AfFtnAA/E94C at different concentrations on Cu substrate. (e) AFM characterization of AfFtnAA/E94C at high concentration on Cu substrate.

conditions (Fig. 3b). With the increase in concentration, the small aggregates moved closer to each other, and the cube-shape analogues started to appear (Fig. 3c). At concentration of 0.9 mg $ml^{-1}$, the complete cube-shaped structures were observed (Fig. 3d). To gain more insights into the structural aspect, AFM with a non-contacting mode (NCM) was utilized to further characterize the height of higher-order structures on copper substrate. The height of the assembly on the copper substrate is about 300 nm (Fig. 3e). The morphology of the assembly is cube-like, which is in good agreement with the above results obtained by SEM. The control group composed of AfFtnAA group freeze dried in the same condition, lacks the distinct structures and appeared to have amorphous morphology as expected (Fig. 3a).

### Assembly mechanism

To elucidate the assembly mechanism, Raman spectroscopy was applied to characterize the interaction between the copper template and AfFtnAA/E94C (Fig. 4). Cysteine can be found in three major states that are the cysteine coordinated with copper, cystines (*i.e.*, disulfide bridges), and free cysteines.[31] In the copper-coordinated cystein, the peak in the spectral region below 500 $cm^{-1}$ corresponds to the metal-S stretching modes, which proved copper inducing of the assembly. In the conjugated cysteine, the signal in the spectral region between 550 $cm^{-1}$ and 500 $cm^{-1}$ was observed, falling in the region generating information on disulfide bridges. In addition, the amide bond region in the Raman spectrum was also investigated to provide more evidence about the S–S state. The peak in the spectral region between 800 $cm^{-1}$ and 600 $cm^{-1}$ corresponds to the C–S stretching modes. These results on cysteine-copper analyses are consistent with previous work.[32] Together, the results explain the influence of copper substrate on AfFtnAA/E94C assembly.

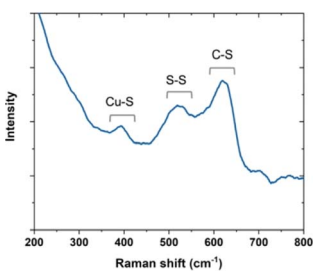


Fig. 4 Raman curve of AfFtnAA/E94C on Cu substrate *via* freeze dry.

To further explain the influence of copper substrate during the assembly process, the same protein, AfFtnAA/E94C, was assembled on a different substrate, Si wafer, under the same condition and the same method, freeze drying (Fig. S3†). Small fragments were observed at low concentration conditions (Fig. S3b†). The increase in concentration led to agglomeration of small aggregates and diamond-shaped analogues started to appear (Fig. S3c†). Eventually, the complete diamond-shaped structures appeared when the concentration reached 0.9 mg $ml^{-1}$ (Fig. S3d†). AFM was also applied to characterize the height of the assembly on the silicon substrate. As shown in Fig. S4,† the height of the assembly on the silicon substrate is about 300 nm. The morphology of the assembly is diamond-shape, which is consistent with the SEM results. AfFtnAA group was freeze dried on the silicon substrate as well, serving as the control group. As shown in Fig. S3a,† amorphous morphology was detected. The different morphologies between Cu substrate group and Si substrate group suggest that substrates can influence the formation of the morphology of AfFtnAA/E94C morphologies, which further supports the important role that substrates and templates play during the construction of the assemblies.

### HER performance of AfFtnAA/E94C assembly

Ferritin has been explored for a wide range of applications in biotechnology including nanodevices,[33] contrast agents for medical imaging,[34] drug delivery,[35] and vaccines.[36] However, the functional analysis of ferritin-based assembly is still in the initial stage. Our group has shown the potential of ferritins to be incorporated into material with electrical properties, including memristors[33] and electrocatalysis in fuel cells.[37] Motivated by

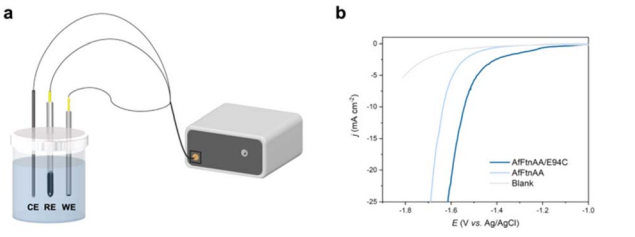


Fig. 5 (a) Schematic of the three-electrode cell system for HER characterization. The reference electrode is Ag/AgCl. The counter electrode is carbon rod. A glassy carbon electrode coated with samples is the working electrode. (b) LSV curves of AfFtnAA/E94C and AfFtnAA freeze-dried on Cu substrate.

these works, linear sweep voltammetry (LSV) of AfFtnAA/E94C assembly on the copper substrate was characterized to determine the HER performance. The measurement was conducted on an electrochemical workstation adopting the three-electrode cell system (Fig. 5a). A glassy carbon electrode coated with freeze dried samples was utilized as the working electrode. Ag/AgCl electrode was selected as the reference electrode. Carbon rod served as the counter electrode. The HER performances were assessed in phosphate buffer (PBS). An empty glassy carbon electrode served as blank control. For comparative purposes, the AfFtnAA, the closed-pore AfFtn without cysteine mutation, was freeze-dried on other Cu substrates and used as working electrodes. Fig. 5b shows the $iR_{initial}$-compensated LSV curves of AfFtnAA/E94C (freeze dried on Cu substrate), AfFtnAA (freeze dried on Cu substrate), and the blank glassy carbon electrode. Over the entire potential range, the current density of AfFtnAA/E94C group is much higher than those of the AfFtnAA group and blank control, suggesting the assembled AfFtnAA/E94C has better HER activity than the amorphous samples of AfFtnAA and the blank glassy carbon electrode. At −1.6 V, the current density of AfFtnAA/E94C is $-21.4$ mA cm$^{-2}$, which is 3.8 times higher than that of AfFtnAA ($-5.6$ mA cm$^{-2}$). The results indicate the unique advantage of HER performances correlated of higher-order structures based on AfFtnAA/E94C in contrast to the amorphous samples of AfFtnAA. The most advanced and widely used component for HER catalysis, platinum, possesses outstanding HER performance resulted from the moderate ability of adsorption and desorption of the hydrogen at the surface of platinum.[26] However, due to the different physical and chemical properties of inorganic and organic components, it is difficult to directly compare the HER activity between platinum and protein-cage-based materials. Although platinum has good corrosive resistance, the HER performance of platinum in neutral condition is not that satisfactory.[26] In contrast, biomacromolecules has good stability in neutral condition. Moreover, compared with platinum, which is scarce in nature and high-cost,[26] protein cages are natural components and can be produced and purified with low-cost and simple method. This work shows the potential of utilizing biomaterials for electrochemical applications in neutral condition that can be explored as substituents of Pt-based electrocatalyst for HER performance.

# Conclusions

In this study, we successfully constructed higher-order assemblies on copper substrate using mutated ferritin, AfFtnAA/E94C, as building blocks. The presence of cysteine on the surface of the cage was shown to be instrumental to the assembly formation by serving as the active moiety for binding with copper substrate. We characterized the morphology *via* SEM and AFM and found that only AfFtnAA/E94 samples resulted in cube-shape structure. Using Raman spectroscopy, we determined the mechanism of the assembly to be copper-induced. Functional characterization showed that HER performance of the copper-assembled AfFtnAA/E94C is 3.8 times higher compared to the amorphous samples of AfFtnAA group at −1.6 V. The observations suggest that the higher-order structures composed of AfFtnAA/E94C contribute to the improvement of HER behavior. However, there remains a gap between the HER performance of the assembly of ferritins in this study and that of commercially applied Pt catalysts. Developing new assembly methods and finding new protein cage units to obtain protein cage assemblies with better electrochemical properties are required for future improvements. Taking advantage of protein-cage-based materials properties and the limited investigation of HER activity of protein-cage-based materials, this work provides fresh insights into electrocatalytic behaviors of protein-based materials and seek future developments and applications for higher-order structures based on protein cages.

# Experimental

### Expression and purification of AfFtnAA and related variants

**Expression of AfFtnAA and related variants.** The AfFtnAA gene was in pET11a vector and expressed in the BL21(De3) C+RIL. The overexpression and protein purification were conducted as previously reported method.[29] Ampicillin and Chloramphenicol of a final concentration of 100 μg ml$^{-1}$ and 50 μg ml$^{-1}$ were added. A 40 ml preculture was incubated for ∼17 hours. Culture in 4 L volume was grown in lysogeny broth (LB) media at 37 °C with shaking until the optical density (OD600) reached 0.6–0.8. Isopropyl β-D-1-thiogalactopyranoside (IPTG) at final concentration of 1 mM was added. The cultures were then shaken at 37 °C for 4 hours and the cells were harvested by centrifugation and stored at −40 °C prior to further use.

**Purification of AfFtnAA and related variants.** The frozen cells were resuspended in resuspension buffer (25 mM HEPES, 50 mM NaCl, pH 7.4). The suspension was then sonicated on ice for 45 min with 5-second ON/OFF. Lysed cells were placed in water bath at 80 °C for 10 min, centrifuged at 193 000×*g* for 60 min at 4 °C, and filtered with 0.22 μm filter. Ammonium sulphate was added afterwards. The clear supernatant was then purified using one HiPrep Phenyl FF (high sub) column, which were equilibrated with equilibration buffer (25 mM HEPES, 50 mM NaCl, 500 mM ammonium sulphate, pH 7.4), and the protein was eluted using the elution buffer (25 mM HEPES, 50 mM NaCl, pH 7.4). Selected fractions containing the protein of interest were then stored at 4 °C for further usage. The concentration of apo AfFtnAA were quantified using Bradford Assay. The proteins were diluted to 0.3 mg ml$^{-1}$ with resuspension buffer (25 mM HEPES, 50 mM NaCl, pH 7.4). Fe at ∼400 atoms were added to apo proteins twelve separate times (4800 Fe total) followed by incubation at room temperature. The proteins were then transferred to 4 °C and incubated overnight. Fe-loaded ferritins were centrifuged at 12 000×*g* for 5 min to remove precipitates. The supernatant was collected and passed through HiPrep 26/10 Desalting column in desalting buffer (25 mM HEPES, 50 mM NaCl, pH 7.4) to remove the excess Fe.

### Characterizations of individual protein cages

**Dynamic light scattering (DLS).** The hydrodynamic diameter of the protein samples were measured using Malvern Nano-ZS

Zeta Sizer. Sample of 1 ml volume in buffer (25 mM HEPES, 50 mM NaCl, pH 7.4) was placed in plastic cuvette. The measurement was taken at 25 °C in triplicate.

**Matrix-assisted laser desorption/ionization time-of-flight (MALDI-TOF) mass spectrometry.** To determine the molecular mass, the samples were embedded in MBT matrix without saturator or additives. The measurements were performed at central facility using MALDI TOF/TOF ABI 4800.

**Transmission electron microscopy (TEM).** Electron micrographs of the protein cages were obtained using Tecnai-12 (T12) iCorr-120 kV TEM. Samples were negatively stained with 2% uranyl acetate and air dried before loading to the sample holder and imaged at 120 kV.

#### Characterizations of the assembly based on protein cages

**Field emission scanning electron microscope (FESEM).** The morphologies of the assemblies were observed using JEOL JSM 6700F SEM. Samples were coated with platinum at 20 mA current for 120 s.

**Atomic force microscopy (AFM).** Park NX10 Atomic Force Microscope was applied to characterize the morphologies of assemblies. XEI software was utilized to analyse and process the AFM data.

**Raman spectroscopy.** Raman spectra were collected on a Renishaw InVia reflex Raman spectrometer using a 785 nm laser and a 20× objective.

**Electrochemical measurements.** Linear sweep voltammetry with IR compensation was performed on an electrochemical workstation (CHI 660D) and undertaken at a sweep rate of 5 mV $s^{-1}$. The working electrode was glassy carbon electrode (diameter: 3 mm, area: 0.071 $cm^2$).

## Author contributions

S. L. and R. S. conceived and designed the project. R. S. carried out experiments. All authors contributed to writing and editing the manuscript.

## Conflicts of interest

There are no conflicts to declare.

## References


1 Y. Bai, Q. Luo and J. Liu, Protein self-assembly via supramolecular strategies, *Chem. Soc. Rev.*, 2016, **45**(10), 2756–2767.

2 Q. Luo, C. Hou, Y. Bai, R. Wang and J. Liu, Protein assembly: versatile approaches to construct highly ordered nanostructures, *Chem. Rev.*, 2016, **116**(22), 13571–13632.

3 K. Liu, Y. Kang, Z. Wang and X. Zhang, 25th anniversary article: Reversible and adaptive functional supramolecular materials:"Noncovalent interaction" matters, *Adv. Mater.*, 2013, **25**(39), 5530–5548.

4 R. Sun and S. Lim, Protein cages as building blocks for superstructures, *Eng. Biol.*, 2021, 35–42.

5 G. n. Jutz, P. van Rijn, B. Santos Miranda and A. Böker, Ferritin: a versatile building block for bionanotechnology, *Chem. Rev.*, 2015, **115**(4), 1653–1701.

6 W. Roos, I. Ivanovska, A. Evilevitch and G. Wuite, Viral capsids: mechanical characteristics, genome packaging and delivery mechanisms, *Cell. Mol. Life Sci.*, 2007, **64**, 1484–1497.

7 U. Zügel and S. H. Kaufmann, Role of heat shock proteins in protection from and pathogenesis of infectious diseases, *Clin. Microbiol. Rev.*, 1999, **12**(1), 19–39.

8 W. M. Aumiller, M. Uchida and T. Douglas, Protein cage assembly across multiple length scales, *Chem. Soc. Rev.*, 2018, **47**(10), 3433–3469.

9 C. Lv, X. Zhang, Y. Liu, T. Zhang, H. Chen, J. Zang, B. Zheng and G. Zhao, Redesign of protein nanocages: the way from 0D, 1D, 2D to 3D assembly, *Chem. Soc. Rev.*, 2021, **50**(6), 3957–3989.

10 Z. Wang, H. Gao, Y. Zhang, G. Liu, G. Niu and X. Chen, Functional ferritin nanoparticles for biomedical applications, *Front. Chem. Sci. Eng.*, 2017, **11**, 633–646.

11 K. Zhou, H. Chen, S. Zhang, Y. Wang and G. Zhao, Disulfide-mediated reversible two-dimensional self-assembly of protein nanocages, *Chem. Commun.*, 2019, **55**(52), 7510–7513.

12 V. Liljeström, J. Mikkilä and M. A. Kostiainen, Self-assembly and modular functionalization of three-dimensional crystals from oppositely charged proteins, *Nat. Commun.*, 2014, **5**(1), 1–9.

13 M. A. Kostiainen, O. Kasyutich, J. J. Cornelissen and R. J. Nolte, Self-assembly and optically triggered disassembly of hierarchical dendron–virus complexes, *Nat. Chem.*, 2010, **2**(5), 394.

14 M. A. Kostiainen, C. Pietsch, R. Hoogenboom, R. J. Nolte and J. J. Cornelissen, Temperature-Switchable Assembly of Supramolecular Virus–Polymer Complexes, *Adv. Funct. Mater.*, 2011, **21**(11), 2012–2019.

15 M. A. Kostiainen, P. Hiekkataipale, A. Laiho, V. Lemieux, J. Seitsonen, J. Ruokolainen and P. Ceci, Electrostatic assembly of binary nanoparticle superlattices using protein cages, *Nat. Nanotechnol.*, 2013, **8**(1), 52.

16 A. Korpi, C. Ma, K. Liu, Nonappa, A. Herrmann, O. Ikkala and M. A. Kostiainen, Self-assembly of electrostatic cocrystals from supercharged fusion peptides and protein cages, *ACS Macro Lett.*, 2018, **7**(3), 318–323.

17 P. A. Sontz, J. B. Bailey, S. Ahn and F. A. Tezcan, A metal organic framework with spherical protein nodes: rational chemical design of 3D protein crystals, *J. Am. Chem. Soc.*, 2015, **137**(36), 11598–11601.

18 J. B. Bailey, L. Zhang, J. A. Chiong, S. Ahn and F. A. Tezcan, Synthetic modularity of protein–metal–organic frameworks, *J. Am. Chem. Soc.*, 2017, **139**(24), 8160–8166.

19 M. Künzle, T. Eckert and T. Beck, Metal-assisted assembly of protein containers loaded with inorganic nanoparticles, *Inorg. Chem.*, 2018, **57**(21), 13431–13436.

20 E. J. Lee, N. K. Lee and I.-S. Kim, Bioengineered protein-based nanocage for drug delivery, *Adv. Drug Deliv. Rev.*, 2016, **106**, 157–171.

21 W. Shan, H. Zheng, G. Fu, C. Liu, Z. Li, Y. Ye, J. Zhao, D. Xu, L. Sun and X. Wang, Bioengineered nanocage from HBc protein for combination cancer immunotherapy, *Nano Lett.*, 2019, **19**(3), 1719–1727.
22 M. Sarker, N. Tomczak and S. Lim, Protein nanocage as a pH-switchable Pickering emulsifier, *ACS Appl. Mater. Interfaces*, 2017, **9**(12), 11193–11201.
23 L. Zhang, J. B. Bailey, R. H. Subramanian, A. Groisman and F. A. Tezcan, Hyperexpandable, self-healing macromolecular crystals with integrated polymer networks, *Nature*, 2018, **557**(7703), 86–91.
24 J. B. Bailey and F. A. Tezcan, Tunable and cooperative thermomechanical properties of protein–metal–organic frameworks, *J. Am. Chem. Soc.*, 2020, **142**(41), 17265–17270.
25 S. Chakraborti, A. Korpi, M. Kumar, P. Stepien, M. A. Kostiainen and J. G. Heddle, Three-dimensional protein cage array capable of active enzyme capture and artificial chaperone activity, *Nano Lett.*, 2019, **19**(6), 3918–3924.
26 J. Zhu, L. Hu, P. Zhao, L. Y. S. Lee and K.-Y. Wong, Recent advances in electrocatalytic hydrogen evolution using nanoparticles, *Chem. Rev.*, 2019, **120**(2), 851–918.
27 S. K. Patel, D. Das, S. C. Kim, B.-K. Cho, V. C. Kalia and J.-K. Lee, Integrating strategies for sustainable conversion of waste biomass into dark-fermentative hydrogen and value-added products, *Renew. Sustain. Energy Rev.*, 2021, **150**, 111491.
28 B. Sana, E. Johnson, P. Le Magueres, A. Criswell, D. Cascio and S. Lim, The role of nonconserved residues of Archaeoglobus fulgidus ferritin on its unique structure and biophysical properties, *J. Biol. Chem.*, 2013, **288**(45), 32663–32672.
29 B. Sana, E. Johnson and S. Lim, The unique self-assembly/disassembly property of Archaeoglobus fulgidus ferritin and its implications on molecular release from the protein cage, *Biochim. Biophys. Acta, Gen. Subj.*, 2015, **1850**(12), 2544–2551.
30 S. Ravishankar and S. Lim, Cyclodextrin conjugated ferritin nanocages reduce intracellular cholesterol level in foam cells, *Nano Res.*, 2019, **12**, 2925–2932.
31 A. Torreggiani and A. Tinti, Raman spectroscopy a promising technique for investigations of metallothioneins, *Metallomics*, 2010, **2**(4), 246–260.
32 J. S. Calvo, R. L. E. Villones, N. J. York, E. Stefaniak, G. E. Hamilton, A. L. Stelling, W. Bal, B. S. Pierce and G. Meloni, Evidence for a long-lived, Cu-coupled and oxygen-Inert disulfide radical anion in the assembly of metallothionein-3 Cu (I) 4-thiolate cluster, *J. Am. Chem. Soc.*, 2022, **144**(2), 709–722.
33 F. Meng, L. Jiang, K. Zheng, C. F. Goh, S. Lim, H. H. Hng, J. Ma, F. Boey and X. Chen, Protein-Based Memristive Nanodevices, *Small*, 2011, **7**(21), 3016–3020.
34 B. Sana, C. L. Poh and S. Lim, A manganese–ferritin nanocomposite as an ultrasensitive T 2 contrast agent, *Chem. Commun.*, 2012, **48**(6), 862–864.
35 Z. Zhen, W. Tang, H. Chen, X. Lin, T. Todd, G. Wang, T. Cowger, X. Chen and J. Xie, RGD-modified apoferritin nanoparticles for efficient drug delivery to tumors, *ACS Nano*, 2013, **7**(6), 4830–4837.
36 M. Kanekiyo, C.-J. Wei, H. M. Yassine, P. M. McTamney, J. C. Boyington, J. R. Whittle, S. S. Rao, W.-P. Kong, L. Wang and G. J. Nabel, Self-assembling influenza nanoparticle vaccines elicit broadly neutralizing H1N1 antibodies, *Nature*, 2013, **499**(7456), 102–106.
37 H. Qiu, X. Dong, B. Sana, T. Peng, D. Paramelle, P. Chen and S. Lim, Ferritin-templated synthesis and self-assembly of Pt nanoparticles on a monolithic porous graphene network for electrocatalysis in fuel cells, *ACS Appl. Mater. Interfaces*, 2013, **5**(3), 782–787.